



Contents lists available at ScienceDirect

Journal of Organometallic Chemistry

journal homepage: www.elsevier.com/locate/jorganchem

Tetraphosphines with tetra(biphenyl)silane and -stannane cores as rigid scaffold linkers for immobilized catalysts

Joseph H. Baker, Nattamai Bhuvanesh, Janet Blümel*

Department of Chemistry, Texas A&M University, P.O. Box 30012, College Station, TX 77842-3012, USA

ARTICLE INFO

Article history:

Received 8 February 2017

Received in revised form

15 March 2017

Accepted 16 March 2017

Available online xxx

ABSTRACT

The silane $\text{Si}(p\text{-C}_6\text{H}_4\text{-}p\text{-C}_6\text{H}_4\text{Br})_4$ and the stannane $\text{Sn}(p\text{-C}_6\text{H}_4\text{-}p\text{-C}_6\text{H}_4\text{Br})_4$ have been synthesized and characterized. For the silane a single crystal X-ray structure has been obtained. Tetralithiation of the silane with ${}^t\text{BuLi}$ and quenching with the corresponding chlorophosphines gave the tetraphosphines $\text{Si}(p\text{-C}_6\text{H}_4\text{-}p\text{-C}_6\text{H}_4\text{PR}_2)_4$ with ($\text{R} = \text{Ph}, \text{Cy}, {}^i\text{Pr}, {}^t\text{Bu}$). Tetralithiation of $\text{Sn}(p\text{-C}_6\text{H}_4\text{-}p\text{-C}_6\text{H}_4\text{Br})_4$ led to cleavage of the Sn–C bonds. Therefore, $\text{Sn}(p\text{-C}_6\text{H}_4\text{-}p\text{-C}_6\text{H}_4\text{PPh}_2)_4$ was synthesized by Br/Li exchange of $p\text{-Br-C}_6\text{H}_4\text{-}p\text{-C}_6\text{H}_4\text{PPh}_2$ with ${}^t\text{BuLi}$ and reaction with SnCl_4 . The silanes have been immobilized on silica by generating three phosphonium groups per molecule that were bound to the surface via strong electrostatic interactions. The remaining phosphine group was subsequently coordinated to Wilkinson's catalyst via ligand exchange. All solids have been characterized by quantitative ${}^{31}\text{P}$ solid-state NMR spectroscopy. The catalysts, immobilized via the tetraphosphine linker scaffolds with biphenyl spacers, showed high activities and selectivities with respect to the hydrogenation of 1-dodecene. They have been recycled 9 times in a batchwise manner. All immobilized catalysts eventually formed rhodium nanoparticles that retained their catalytic activity even after being exposed to air.

© 2017 Elsevier B.V. All rights reserved.

1. Introduction

Catalysis represents one of the most central aspects of chemistry. Unfortunately, the “ideal catalyst” [1] with eternal lifetime, superior activity and total selectivity has still not been discovered. Therefore, different approaches have been investigated to improve the removal and recyclability of originally homogeneous catalysts. For example, one successful approach is based on biphasic catalysis using two liquid phases, one fluoruous and one conventional organic phase, and controlling their miscibility via temperature under different conditions [2]. In another approach a rhodium catalyst could successfully be adsorbed on a teflon tape and reversibly released into solution for performing as a homogeneous catalyst [3].

Our group and others have successfully pursued the immobilization of catalysts on solid supports via diverse linkers [4]. Optimally, an immobilized catalyst retains all the qualities of the homogeneous analog, while it allows for easy catalyst separation from the reaction mixture, batchwise recycling, or application in a

continuous flow setting.

After experimenting with zirconium phosphate nanoplatelets [5] and various other oxides as support [6], silica [7] remains the most favorable support for immobilized catalysts. Silica can easily be modified with linkers incorporating ethoxysilane groups [8,9], it is mechanically robust, stable at higher temperatures, and settles within minutes after the reaction, so that the supernatant containing the products can simply be decanted. After washing the silica, the covalently bound immobilized catalyst can be used for the next catalytic run.

Using bifunctional phosphine linkers incorporating ethoxysilane groups, immobilized nickel catalysts for cyclotrimerization [10], palladium and copper catalyst systems for Sonogashira reactions [11], and rhodium catalysts for olefin hydrogenation [12] have been generated. All these catalysts showed unprecedented activities and lifetimes and could be recycled many times.

Nevertheless, some problems remain. For example, neighboring catalyst molecules on the surface can dimerize or agglomerate. Wilkinson's catalyst readily dimerizes already when stirred at room temperature in benzene [13], and the dimer is catalytically not active. Accordingly, it was found that diluting the immobilized Wilkinson-type catalysts on the surface improved the catalytic performance substantially [12b,c]. However, diluting surface-

Dedicated to Prof. Dr. John Gladysz on the occasion of his 65th birthday.

* Corresponding author.

E-mail address: bluemel@tamu.edu (J. Blümel).

bound species entails a relative increase in the bulk of the support material, which is an unpopular scenario in industrial settings. Another, fatal problem arises when linkers decompose upon reaction with silica [14]. Additionally, phosphine linkers incorporating ethoxysilane groups can be transformed into the corresponding ethylphosphonium salts at higher temperatures, which are no longer able to coordinate to metal complexes [15]. The detachment of the catalyst complex from monodentate linkers, a general problem for immobilized catalysts which is typically classified as “leaching”, leads to the gradual loss of metal complexes. We have investigated this issue using palladium complexes by solid-state NMR and found that this problem can only be ameliorated by using favorable chelate linkers [11b,c]. Finally, homogeneous catalysts that are tethered to the support via linkers with flexible alkyl chains can reach the support surface and decompose or form nanoparticles [5,12a].

Recently, we have explored a rigid tetraphosphine linker system with tetraphenylelement cores [16] that successfully prevented rhodium catalysts from dimerizing and kept the metal centers at a safe distance from the reactive silica surface [17]. Indeed, Wilkinson-type rhodium catalysts with unprecedented activity and selectivity could be obtained by using the rigid tetrahedral linker $\text{Sn}(p\text{-C}_6\text{H}_4\text{PPh}_2)_4$ [17].

In this contribution we extend the rigid linker theme and explore whether using the longer biphenyl instead of phenyl units will further improve the immobilized catalysts by preventing dimerization and decomposition by contact with the surface, as the distance between the substituents at the linker should increase from about 10 to 15 Å. For this purpose, diverse new tetraphosphines with tetra(biphenyl)element cores have been synthesized and fully characterized. They have been immobilized on silica and Wilkinson-type rhodium catalysts have been coordinated.

Selected linkers have been tested for their activity and recyclability in the important catalytic olefin hydrogenation [18] because there is already a substantial body of data on rhodium-catalyzed hydrogenation from our group [12,17]. A comparison with the hydrogenation results of other groups, using different catalytic systems, will be interesting as well [19]. Special interest in the work described here is placed on a linker with a silicon atom at the core instead of a tin atom [17] in order to exclude the participation of the center atom of the linker in the catalytic hydrogenation.

Besides our application as linkers for immobilized catalysts, tetrahedral scaffold-type molecules are also of general interest in other fields. For example, they function as rigid structural elements for metal organic frameworks (MOFs) [20], porous organic and aromatic frameworks (POFs, PAFs) [21] and dendrimers [22]. Furthermore, they are of interest for studying photochemical effects [23], and for materials chemistry in general [24].

The most powerful method for characterizing amorphous solids is solid-state NMR spectroscopy [25]. It has been an invaluable tool for characterizing covalently bound linkers, catalysts, and supports, and recently the dynamics of surface-adsorbed solid metal complexes could be determined by solid-state NMR analysis [26]. Silica as the support material is very advantageous for solid-state NMR studies as it does not interfere with the measurements as other supports do, for example, alumina containing quadrupolar nuclei [6], or polymers producing ^{13}C NMR background signals.

In this contribution, new tetraphosphines with tetra(biphenyl)silane and -stannane cores will be synthesized, characterized, immobilized, and tested as linkers for immobilized Wilkinson-type rhodium catalysts for olefin hydrogenation.

2. Syntheses of tetra(biphenyl)element compounds

We have previously reported on tetraphosphines with

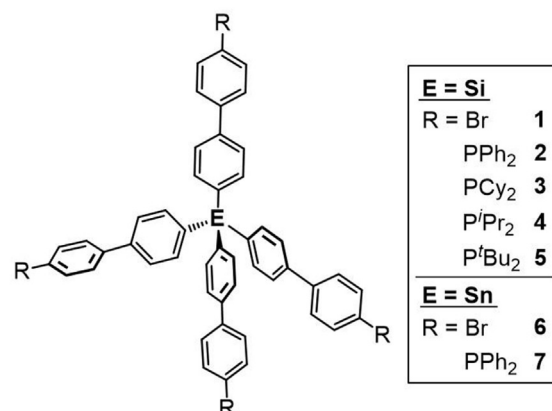
tetraphenylmethane, tetraphenylsilane, and tetraphenylstannane cores [16,17]. In the following the syntheses of the analogs 1–7 (Scheme 1) with tetra(biphenyl)silane and -stannane cores are described. Different strategies for syntheses of rigid tetrahedral aryl systems have been reported in the literature [27], making use of multiple palladium coupling reactions and boronic acid derivatives, as well as Grignard reagents. For the sake of simplicity and to avoid multiple steps in the synthesis, our approach to the biphenyl systems was analogous to the successful previous syntheses of the tetraphenylelement compounds [16,17].

Unfortunately, the syntheses of these tetra(biphenyl)element compounds proved to be more difficult as compared to the previously synthesized molecules with tetraphenylelement cores. When the syntheses of the tetrabromo compounds 1 and 6, the precursors for 2–5 and 7, are pursued according to Scheme 2, the yields are not optimal.

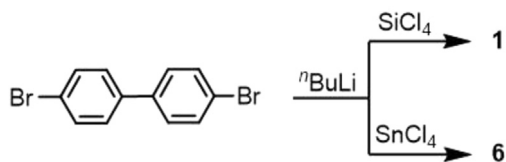
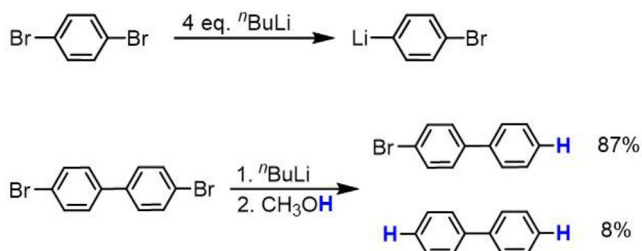
The reason for the lower yields is that 4,4'-dibromobiphenyl can not be monolithiated selectively [28]. In comparison, the monolithiation of 1,4-dibromobenzene is very selective and dilithiation does not even take place when applying an excess of four equivalents of *n*-butyllithium at room temperature (Scheme 3) [29]. The monolithiation of 4,4'-dibromobiphenyl has been described in the literature and often used as a benchmark for the selectivity of a metalation reaction performed with an organolithium or Grignard reagent. However, even with the use of micromixers and temperatures as low as -78°C absolute selectivity has not been achieved [28b]. Scheme 3 presents a typical distribution of mono- versus dilithiated dibromobiphenyl, as determined by quenching with methanol [28b]. This distribution has been reproduced in our hands, and the percentage of monolithiation of 4,4'-dibromobiphenyl is among the highest reported in the literature to the best of our knowledge.

The lack of selectivity of the monolithiation of 4,4'-dibromobiphenyl is problematic considering that the dilithiated biphenyl can lead to oligomers when being reacted with SiCl_4 or SnCl_4 in the next step. This further reduces the yields substantially.

After numerous experiments aimed at ameliorating the outcome of the Br/Li exchange, it could be determined that the best approach was to remove the dilithiated byproduct from the reaction mixture prior to proceeding with the following synthetic steps. Fortunately, the dilithiated biphenyl precipitates out of diethyl ether while the monolithiated biphenyl is soluble in ether at room temperature. Therefore, the separation of the ether solution from the precipitate allows the isolation of the mono- and dilithium salts. Starting from the clean lithium salts limits the amounts of side products formed in subsequent reactions. In order to test the



Scheme 1. Synthesized and characterized tetra(biphenyl)element compounds 1–7.

Scheme 2. Synthesis of **1** and **6**.

Scheme 3. Br/Li exchange products with 1,4-dibromobenzene and 4,4'-dibromobiphenyl (5% remaining starting material).

quality of the separation by the solubility in ether, the precipitate was quenched with water. The resulting ^1H and ^{13}C NMR spectra of the water-quenched precipitate show that it consisted of pure dilithium salt. The signals in the spectra perfectly match the literature values for biphenyl [30]. The unoptimized yield of the isolated compound after the lithiation was 19%.

Removal of the dilithiated biphenyl prior to subsequent synthesis steps proved to be extremely beneficial for generating the tetrabromo compound **1** (Scheme 1). The compound was obtained with high purity in 88% yield. The product could be crystallized by slow evaporation of acetone producing clear needle-like crystals with high enough quality to subject them to single crystal X-ray analysis (Fig. 1) [31]. There are two distinct molecules in the unit cell which matches the ^{29}Si solid-state NMR spectrum of polycrystalline **1**, which shows two isotropic lines at -14.7 and -15.7 ppm, representing each molecule in the unit cell. This corresponds nicely with our earlier results on tetra(*p*-bromophenyl)silane [17].

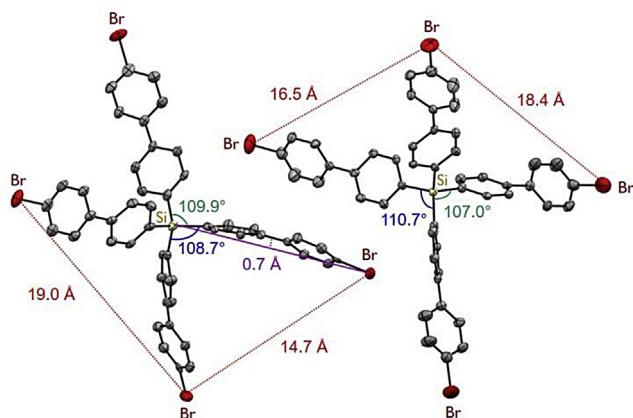
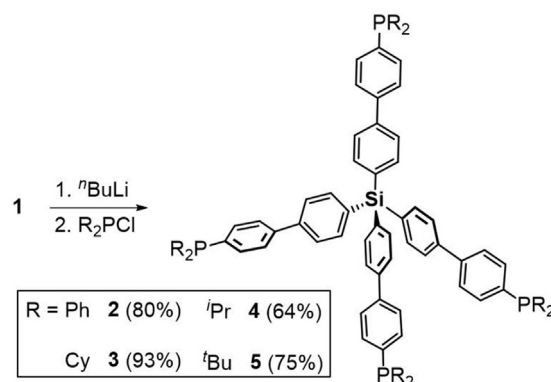
It is interesting to note the very obvious high degree of bending in the biphenyl spokes in the molecules that is most probably enforced by the strain of packing in the crystal lattice (Fig. 1). In one case, the deviation from linearity amounts to 0.7 \AA (Fig. 1, left). This

feature is reminiscent of the bending of the conjugated polyyne chains described earlier in the context of “molecular wires” [32].

The bends in **1** create significant changes in the distances between the four bromine atoms in each molecule. The two that are bent towards each other are 14.7 \AA apart, whereas the two that are bent away from each other are 19.0 \AA apart. The bending even affects the lengths of the biphenyl units, for example, it shortens the length of one “arm” from 10.87 \AA on the left to 10.84 \AA on the right. It should be noted that in the only other literature known crystal structure of a tetra(biphenyl)silane [33] the bends are smaller. Due to the strains in the crystal lattice, the deviations from the ideal tetrahedral angle of 109.5° are substantial. For example, the right molecule in Fig. 1 shows two deviating values of 107.0° and 110.7° . This leads again to very different distances between the bromine atoms within one molecule, 18.4 versus 16.5 \AA . The tight packing of the molecules within the crystal lattice results in a comparatively high density of the crystal of 1.58 g/cm^3 . Finally, with respect to using these tetrahedral scaffolds as linkers for immobilizing catalysts, it should be noted that they will not clog the large pores of the silica used in the presented studies, which are on average 40 \AA in diameter.

Four new tetraphosphines with tetra(biphenyl)silane cores (**2–5**) could be synthesized from **1** in high yields (Scheme 4). For the tetralithiation of **1** with ether as the solvent, the number of equivalents of $^n\text{BuLi}$ had to be increased to 20. This excess proved necessary because even 8 equivalents, an amount that had successfully been used previously with the tetraphenyl core linkers [17], produced a mixture of starting bromides and phosphines after quenching the reaction with the chlorophosphines at $-78\text{ }^\circ\text{C}$. The incomplete tetralithiation was proven by ^{13}C NMR after allowing the reaction mixture to warm to room temperature and stirring for 3 h. Most diagnostic for this purpose was the ^{13}C NMR signal of the nucleus bound to Br at about 122 ppm . In THF the lithiation proceeds much more rapidly and a significantly smaller amount of $^n\text{BuLi}$ is needed, which is more atom economic and beneficial for the subsequent purification.

After quenching the tetralithium species with the corresponding chlorophosphines, the products **2–5** (Scheme 4) could easily be isolated in high purities and yields by removing the solvent, adding ethanol to the residue, filtering the suspension through a frit and thoroughly washing the solid product with ethanol. Fig. 2 displays the solution ^{31}P NMR spectra of the tetraphosphines **2–5** in CDCl_3 . Noteworthy is the absence of phosphorus-containing sideproducts, and that the phosphines are only moderately sensitive towards oxidation and can tolerate chlorinated solvents. Furthermore, there is only one signal for each tetraphosphine, confirming the

Fig. 1. Single crystal X-ray structure of **1**. Two independent molecules are displayed [31].Scheme 4. Synthesis of the tetraphosphines **2–5**.

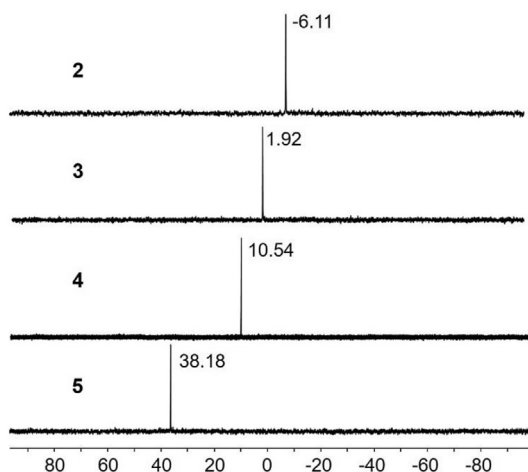


Fig. 2. ^{31}P NMR spectra of tetraphosphines 2–5. Numbers next to the signals correspond to the chemical shift values (ppm).

symmetry of the compounds in solution. None of the signals shows any “fine structure” or additional signals, which would indicate the presence of triphosphines or diphosphines stemming from incomplete Br/Li exchange in the previous step of the synthesis (Scheme 4). It should also be noted that the tetraphosphines 2–5 are rather soluble in organic solvents, excluding the formation of oligomers.

The signal assignments in the ^1H and ^{13}C NMR spectra are straightforward. They are based on the assignments of the tetraphosphines with tetraphenylelement cores reported earlier [16,17], and on various two-dimensional techniques, such as $^1\text{H}, ^1\text{H}$ COSY, and $^{13}\text{C}, ^1\text{H}$ COSY NMR spectra. Fig. 3 shows, for example, the COSY spectrum detailing the assignments of the cyclohexyl ring signals, which are additionally aided by the NMR study of PhPCy_2 reported in the literature [34]. Furthermore, especially with respect to distinguishing the signal sets of the two aryl rings in the biphenyl units, the $^{1-3}J(^{31}\text{P}-^{13}\text{C})$ values are very helpful. The splittings of the carbon NMR signals due to $^{1-4}J(^{31}\text{P}-^{13}\text{C})$ couplings can clearly be seen in the ^{13}C NMR trace in Fig. 3 (left).

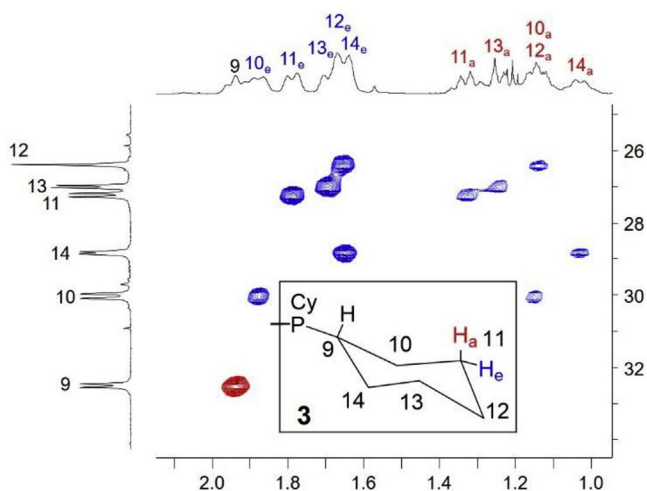


Fig. 3. $^{13}\text{C}, ^1\text{H}$ COSY NMR spectrum of **3** used for signal assignments in the cyclohexyl rings.

3. Synthesis of tetra(biphenyl)stannane scaffolds

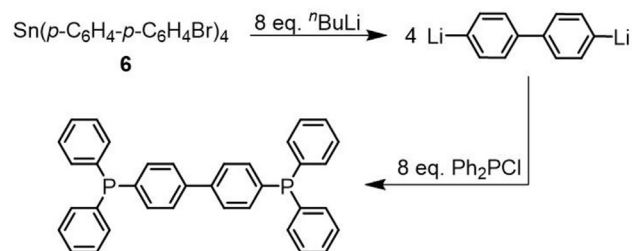
The synthesis of the tin compound **6** (Scheme 1) in analogy to **1** proceeded without difficulties. However, problems were encountered when trying to obtain the tetraphosphine **7** using the synthesis that was successful for **2–5** (Scheme 4). The main problem proved to be that a stoichiometric amount of $^n\text{BuLi}$ only led to incomplete Br/Li exchange. A twofold excess of $^n\text{BuLi}$, however, resulted in the cleavage of the Sn–C bond and formation of dilithiated biphenyl. This is obvious, for example, when the tetrabromide **6** is treated with eight equivalents of $^n\text{BuLi}$, the reaction is quenched with chlorodiphenylphosphine, and 4,4'-bis(diphenylphosphanyl)-1,1'-biphenyl is obtained as the sole phosphorus containing product (Scheme 5). The product has been identified unequivocally by ^{31}P and ^{13}C NMR spectroscopy and ESI MS. To corroborate the attack of the lithiating reagent at the tin center, tetraphenyltin has been subjected to the same treatment with $^n\text{BuLi}$ and chlorodiphenylphosphine, and Ph_2P was found as the sole phosphorus containing product by ^{31}P NMR. Therefore, tetralithiation of **6** is not a viable method for generating **7**, due to the Sn–C bond cleavage under these reaction conditions.

Since the tetralithiation of **6** with the, according to experience, required excess of $^n\text{BuLi}$ [16,17] did not work, other approaches were tested. Unfortunately, addition of tetramethylethylene diamine (TMEDA) to activate the lithiating reagent [35] did not lead to the desired outcome even after varying the stoichiometries and reaction conditions. For example, using 4 equivalents of $^n\text{BuLi}$ only about 50% lithiation was observed. With 6 equivalents about 33% of arylbromides remained, besides decomposed material. Diagnostically most valuable in these attempts proved to be ^{13}C NMR that allowed to identify residual bromoaryl moieties by the C–Br signal at 121.8 ppm.

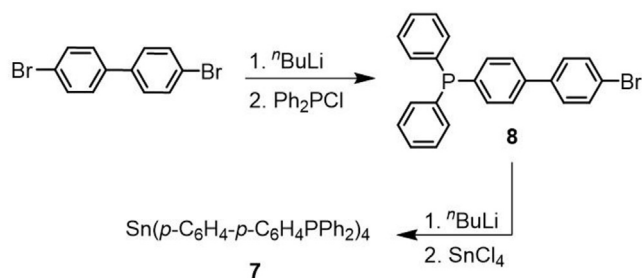
A more successful attempt to synthesize **6** is outlined in Scheme 6. In a first step, the phosphine **8** was prepared in high yields using the protocol for obtaining the clean monolithiated biphenyl described above. The lithiation of **8** with $^n\text{BuLi}$ had to be optimized next. Since triarylphosphines can undergo a P–C bond cleavage with an excess of lithiating reagents, only one equivalent of $^n\text{BuLi}$ was used with **8**. The optimal conditions were identified as the solvent THF, a reaction temperature of $-78\text{ }^\circ\text{C}$, and 1.25 equivalents of TMEDA with respect to $^n\text{BuLi}$. After lithiation of **8** the quench of the reaction mixture with SnCl_4 leads to the tetraphosphine **7** (Scheme 6) in a respectable crude yield of 52%.

4. Immobilization of the tetraphosphine linkers

It has been described previously that phosphines form ethylphosphonium salts with siloxide counteranions in the presence of ethoxysilanes and silica [15b,16,17]. Alkylation of arylphosphines with chloroalkanes does not take place, for example, Ph_3P does not react with the silane used here, 3-chloropropyltriethoxysilane, in



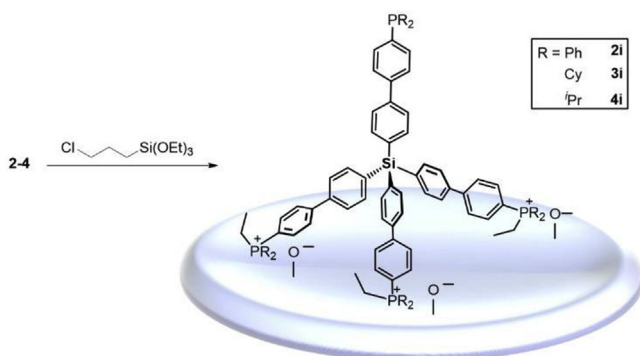
Scheme 5. Generating 4,4'-bis(diphenylphosphanyl)-1,1'-biphenyl by attempted tetralithiation of **6**.



Scheme 6. Syntheses of the tetraphosphine **7** via phosphine **8**.

solution even if the components are stirred in toluene at 90 °C for several days [29]. Furthermore, ethoxysilanes do not react with arylphosphines in solution even under these harsh conditions. The silica surface is needed to activate the ethoxysilanes in order for an ethyl group to be taken up by the phosphine [15a]. Any di-, tri-, or tetraethoxysilane can form ethylphosphonium salts from phosphines in the presence of silica [15b]. As a precursor in the synthesis of other phosphine linkers, chloropropylethoxysilane is readily available in our lab and was used for the immobilization described here. While the transferred ethyl group clearly stems from the ethoxysilyl group, the siloxide counteranion could be associated with the silica surface, or the ethoxysilyl group. The latter is covalently linked to the surface via the residual ethoxy groups, so the linkage of the phosphine might not only be electrostatic in nature, but it could be a combination of electrostatic cation-anion interactions and covalent bonding via the surface-bound ethoxysilyl group. The latter is most likely, as the phosphonium salts are strongly bound to the support surface, and they cannot be washed off the support even by polar organic solvents. It has been demonstrated with quantitative ^{31}P MAS NMR spectroscopy that in the case of tetrahedral tetraphosphine linker scaffolds with tetraphenylelement cores three phosphine groups are transformed into phosphonium groups that are bound to the surface under the right conditions [16,17]. Due to the tetrahedral geometry, one phosphine group cannot react with surface-activated ethoxysilyl groups and remains unchanged, ready to coordinate a metal complex [16,17]. Using this principle, together with the optimized reaction conditions, the tetraphosphines **2–4** have been immobilized successfully to give **2i–4i** as depicted in Scheme 7.

The number of binding phosphonium groups versus phosphine groups in **2i–4i** has been determined by quantitative ^{31}P MAS NMR (Fig. 4). For this purpose, cross-polarization (CP) [25] cannot be applied, because it would give the phosphonium signals an “unfair” boost in signal intensity due to the many alkyl protons in the ethyl groups that provide optimal magnetization transfer. Therefore, the



Scheme 7. Immobilization of **2–4** on silica to generate **2i–4i**.

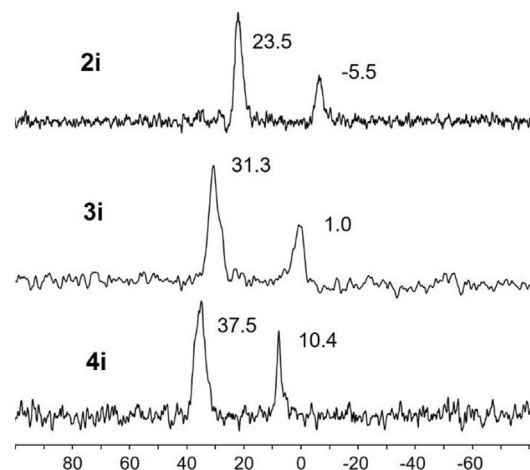


Fig. 4. ^{31}P MAS NMR spectra of the immobilized linkers **2i–4i**. The chemical shifts are given in ppm.

spectra in Fig. 4 have been recorded only with high-power ^1H decoupling and MAS without magnetization transfer, combined with a long relaxation delay of 10 s [16]. The chemical shifts of the downfield phosphonium and upfield phosphine resonances lie within the expected ranges [15–17]. The signal intensity ratios are about 3:1 for the phosphonium and the phosphine signals. The exact values are given in Table 1. Therefore, it can be concluded that the tetraphosphines with tetrabiphenylsilane cores match the immobilization behavior of the previously studied tetraphosphines with tetraphenylsilane and -stannane cores [16,17]. The configuration with three “feet” down and one up, as displayed in Scheme 7 is confirmed.

The surface coverages of **2i–4i** have been obtained by reacting the silica with known specific surface area with an amount of tetraphosphine that creates a submonolayer of molecules on the surface, as estimated by the footprint of the tetrahedral molecules, bound by three “feet”. After the reaction the supernatants have been checked carefully for residual phosphines by ^{31}P NMR. The surface coverages are given in Table 1. They were chosen to lie within the typical range for tetraphosphines with tetraphenylelement cores [16].

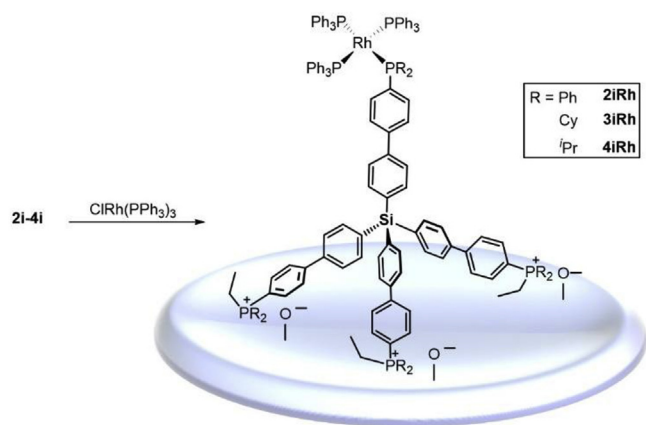
5. Generating immobilized wilkinson-type catalysts

The immobilized Rh complexes **2iRh**, **3iRh** and **4iRh** have been generated from the immobilized linker phosphines **2i**, **3i**, and **4i**, respectively. This has been achieved via ligand exchange by stirring the modified silica with a slight excess of Wilkinson’s catalyst, $\text{CIRh}(\text{PPh}_3)_3$, at room temperature (Scheme 8). Within a few minutes the originally white silica support turns orange while the color of the supernatant is fading. After decanting the supernatant and washing the silica with toluene to remove PPh_3 and excess Wilkinson’s catalyst, the solid is dried *in vacuo* and subjected to ^{31}P solid-state NMR analysis.

The ^{31}P MAS NMR spectra of **2iRh–4iRh** show that no surface-

Table 1
 ^{31}P NMR chemical shifts of resonances from phosphonium (P^+) and phosphine (P) groups, their integral ratios, and surface coverages for **2i–4i**.

Immobilized Species	$\delta(^{31}\text{P}^+)$	$\delta(^{31}\text{P})$	Ratio $\text{P}^+:\text{P}$	Molecules per 100 nm ²
2i	23.5	−5.5	3:1.3	2.9
3i	31.3	1.0	3:1.5	4.7
4i	37.5	10.4	3:1.1	4.0



Scheme 8. Immobilized catalysts **2iRh-4iRh**, generated from **2i-4i** by ligand exchange with Wilkinson's catalyst.

adsorbed PPh_3 [29] is left in the silica. This can, for example, be seen in Fig. 5. Furthermore, the signals of the uncoordinated phosphines vanish when the complexes are bound. This can clearly be seen for **3iRh** versus **3i** (Fig. 5), where the signal of the PCy_2 group at 1.0 ppm vanishes upon coordination. Unfortunately, the ^{31}P NMR signals of the bound Wilkinson-type catalyst at about 30 ppm [12d] are overlapping with the phosphonium resonance and are therefore not resolved. However, the presence of unwanted side-products, like phosphine oxides, can be excluded, as those resonances [15a,36] would have larger chemical shift anisotropies [25a,b] and their rotational sidebands would show prominently in the spectrum of Fig. 5.

6. Catalytic hydrogenation and recycling

Rigid scaffold-type linkers are favorable for immobilized catalysts because they hold the catalyst at a safe distance from the reactive support surface. In this way, the premature decomposition of the catalyst by contact with the silica surface is prevented. Furthermore, due to the rigid nature of the linkers, the coordinated metal complexes cannot form dimers [13] with neighboring catalysts that would no longer be catalytically active. It has been demonstrated with Wilkinson-type catalysts immobilized via rigid linkers with tetraphenylstannane cores previously that this is a winning concept [17]. These catalysts could be recycled in a batchwise manner for 30 times, and the olefin conversion remained

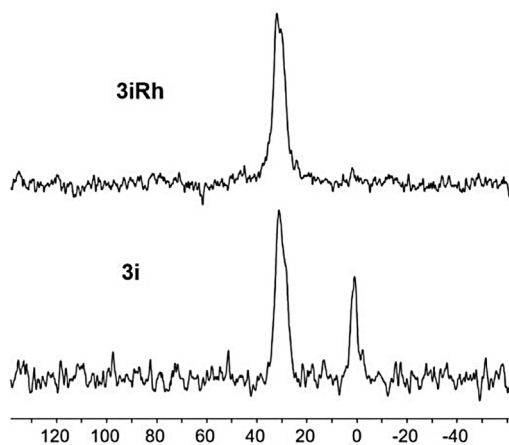


Fig. 5. ^{31}P MAS spectra of **3i** and **3iRh**.

quantitative within a time window of 60 h [17].

Regarding, in comparison, the immobilized catalysts **2iRh-4iRh**, there are three important aspects. (a) The primary question is whether the catalytic performance and especially the longevity improves when the longer biphenyl units are used in the linkers, since the distances to the support and to neighboring catalysts are increased. (b) Furthermore, it is of interest to check whether the record hydrogenation activity reported for the rigid stannane linker reported previously [17] is due in part to the presence of the tin in the center that could function as an activator for hydrogen. Therefore, linkers with silicon in the center that does not influence catalysis are chosen here. (c) Finally, it will be important to see whether the increased distance between the metal centers prevents nanoparticle formation or at least delays its onset. Nanoparticle formation at an early stage of catalysis, due to reduction of Rh(I) to Rh(0) by hydrogen, has been found primarily when using linker systems with flexible alkyl chains [5,12a].

In order to allow for optimal comparability with the previous studies, the same substrate, 1-dodecene, reaction conditions, and hydrogenation apparatus were applied for the catalytic runs [5,12a]. The immobilized catalyst **2iRh** was studied first because it provides a silicon atom in the center and the biphenyl “distance holders”, but leaves the coordination of the rhodium center by triarylphosphine groups in place for a direct comparison with the results in the literature [17].

Fig. 6 shows the results of 1-dodecene hydrogenation with **2iRh**. The data points were collected during each hydrogenation cycle by monitoring the hydrogen gas consumption and recording the volume of H_2 every hour. After each catalytic run, the immobilized catalyst was allowed to settle and the supernatant was removed. The catalyst was subsequently washed with toluene before the next catalytic run was started for checking the batchwise recyclability. Fig. 6 shows that the catalytic activity decreases gradually with every run. However, even in the eighth run the catalytic reaction is completed within 40 h. This performance of **2iRh** is comparable to the results obtained previously [17], but does not exceed expectations. Interestingly, the differences between the completion times are not as pronounced as the ones reported in earlier work using the tetraphenylstannane linker [17].

Overall, at this point regarding question (a) one can safely conclude that the activity and recyclability of the catalyst is similar when using linkers with phenyl versus biphenyl spacers. Perhaps the advantage that the larger distances between the metal centers and to the surface provides is partly diminished by the linkers filling a large portion of the pore space and thus impeding the diffusion of the substrate. This would explain why the reaction is

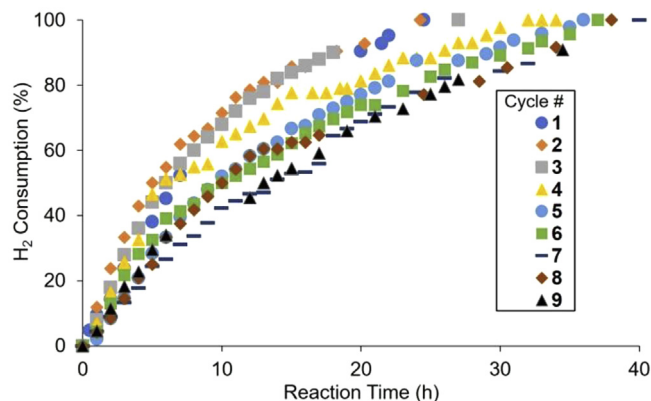


Fig. 6. Percent consumption of H_2 over time for nine batchwise catalytic runs with **2iRh**. The last catalytic run was performed without inert atmosphere.

slower already in the first run as compared to the characteristics found in earlier work [17]. Experiments with silica with larger pores will be necessary to answer this question.

Furthermore, one can tentatively answer question (b), the catalytic activity and recyclability are not influenced in a major way by the tin [17] versus silicon center of the linker.

One of the factors indicating the presence of rhodium nanoparticles is that catalytic activity persists even when oxygen is allowed into the system. This has been described previously for rhodium nanoparticles formed when Wilkinson-type catalysts were immobilized via linkers with long alkyl chains [12a]. When **2iRh** was exposed to oxygen for several hours after the eighth run and used for the catalytic cycle #9 without inert gas atmosphere, the catalytic activity deviate only minimally from the one observed in run 8 (Fig. 6). Therefore, one has to conclude that question (c) can also be answered now. The more extended biphenyl containing linker scaffold does not prevent nanoparticle formation. Taking a close look at the characteristics displayed in Fig. 6 one might speculate that the onset of nanoparticle formation occurs in the fourth run, when the activity transitions into a slower, then persistent mode. This would mean that the onset of nanoparticle formation is delayed for **2iRh**, as nanoparticles already form within the first hours of the initial run for the catalyst tethered with long alkyl chains [12a].

In order to test the influence of alkyl versus aryl substituents at the phosphine groups of the biphenyl linker system, the characteristics of the catalyst **4iRh** with P^iPr_2 groups at the ends of the linker scaffold were investigated. Most importantly, this catalyst needs a reaction temperature of 80 °C before it becomes active. When catalyst **4iRh** is then recycled in a batchwise manner, the activity stays about the same in the first three cycles (Fig. 7). However, in the 4th cycle, the hydrogenation slowed down substantially without obvious reason.

It is noteworthy with respect to point (c) that the material **4iRh** darkened gradually and turned from originally orange to black at the end of the first run (Fig. 8). This indicates the eventual formation of nanoparticles which proceeded faster than for **2iRh**. This might be due to the higher temperature applied, or the nature of the phosphine groups. Again, in order to prove the nanoparticle formation during catalysis, the catalyst was exposed to air after the fourth run. The material remained catalytically as active as in run 4, meaning that no molecular rhodium catalyst that would get deactivated under these conditions remained.

7. Conclusions

Two tetrabromo compounds (**1,6**) and five tetraphosphines (**2–5,7**) with tetra(biphenyl)silane and -stannane cores were

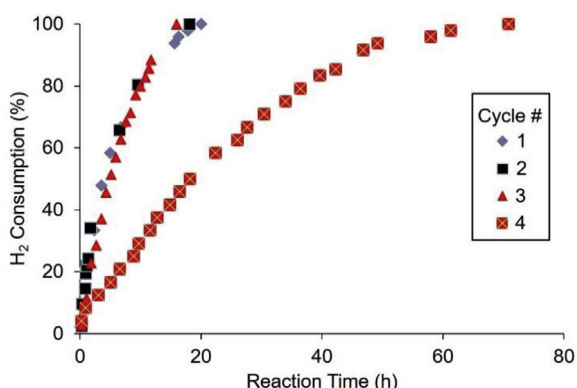


Fig. 7. Hydrogenation of 1-dodecene using the catalyst **4iRh**.



Fig. 8. Images of the catalyst **4iRh** before (left) and after (right) the first hydrogenation cycle. The white spheres are the stirring bar.

synthesized and characterized. Three tetraphosphines were immobilized onto silica (**2i–4i**) and investigated by solid-state NMR. Surface-bound Wilkinson-type rhodium catalysts have been generated by ligand exchange with the immobilized linkers (**2iRh–4iRh**). Catalytic hydrogenation was performed using the catalysts immobilized with **2iRh** and **4iRh**. The former could be recycled at least 9 times without significant loss of activity and the reactions were completed within 40 h. Based on the appearance change of the catalyst and previous results with similar linkers with tetraphenylene cores, the formation of nanoparticles was found. Exposing the used catalyst to air and running another catalytic cycle confirmed the presence of catalytically active rhodium nanoparticles that were inert against oxygen. In future work different pore sizes for the support will be explored in combination with **2iRh** to check whether substrate diffusion slows the catalytic runs. Furthermore, a chelate phosphine group will be attached to the scaffolds which will reduce the detachment of the metal complex as compared to the present monodentate phosphine groups at the linker scaffolds.

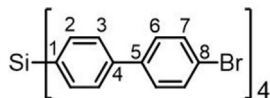
8. Experimental section

All reactions were performed by using standard Schlenk techniques or in a glove-box in an oxygen-free argon atmosphere. The solvents were dried by boiling over Na, distilled and kept under nitrogen. Alternatively, they were obtained from a solvent purification system. All the immobilization experiments were carried out with Merck silica 40 (specific surface area 750 m²/g; average pore size 40 Å; particle size 0.063–0.2 mm) that was dried at 300 °C in *vacuo* (10^{−2} Pa) for at least three days in order to remove adsorbed water and condense surface silanol groups [8].

The ¹H, ¹³C, and ³¹P NMR spectra of molecular compounds were recorded at 499.70, 125.66, and 202.28 MHz on a 500 MHz Varian Inova spectrometer. The ¹³C and ³¹P NMR spectra were measured with ¹H decoupling if not stated otherwise. Neat Ph₂PCL ($\delta(^{31}P) = +81.92$ ppm) in a capillary centered in the 5 mm NMR tubes was used for referencing the ³¹P chemical shifts of the compounds. For referencing the ¹H and ¹³C chemical shifts the residual proton signals of the solvent CDCl₃ and the carbon signal have been used ($\delta(^{1}H) = 7.26$ ppm, $\delta(^{13}C) = 77.00$ ppm). The signal assignments have been obtained by two-dimensional ¹H, ¹H COSY, ¹³C, ¹H HSQC, and ¹³C, ¹H HMBC NMR measurements, and by comparisons with analogous tetraphosphines with tetraphenylene cores [16,17]. All ³¹P solid-state NMR spectra were recorded on a Bruker Avance 400 spectrometer, equipped with a 2.5 mm broadband MAS probehead and ZrO₂ rotors. The modified silica was loosely filled into the rotors under argon in a glove-box. The relaxation delays were 10 s for all surface-immobilized compounds, and the rotational frequency 4 kHz if not mentioned otherwise. High-power decoupling, but no cross-polarization (CP) [25a,c] was applied. All spectra were recorded at room temperature (298 K). The ³¹P MAS NMR spectra were referenced with respect to 85%

H₃PO₄ (aq) by setting the ³¹P NMR peak of solid (NH₄)₂H₂PO₄ as the external standard to +0.81 ppm. For the ²⁹Si NMR spectra the external chemical shift standard Si(SiMe₃)₄ was used.

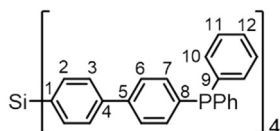
Synthesis of Si(*p*-C₆H₄-*p*-C₆H₄Br)₄ (**1**):



In a 500 ml Schlenk flask, 4,4'-dibromobenzene (2.718 g, 8.71 mmol) dissolved in 300 ml of ether. The solution is cooled to -78 °C and 4.00 ml of 2.5 M ⁿBuLi (10.0 mmol) in hexanes is added dropwise. After allowing the mixture to stir at room temperature for 90 min, the solution is separated from the precipitate via cannula and placed in a different 500 ml Schlenk flask. The flask is cooled to -78 °C and 0.20 ml of SiCl₄ (0.297 g, 1.75 mmol) is added dropwise. The reaction mixture is warmed to room temperature and stirred overnight. The solvent is then removed *in vacuo* and the crude product is redissolved in 80 ml of chloroform. Flash chromatography is then performed with chloroform as the eluent. The solvent is removed *in vacuo* and the powder is washed 3 times with 20 ml of hexanes. Residual solvent is removed *in vacuo* and the product is obtained as white powder in a yield of 88% (1.470 g, 1.54 mmol). Crystals suitable for single crystal X-ray analysis are grown by taking 10 ml of a saturated solution of **1** in acetone, diluting with another 10 ml, and slowly allowing the solvent to evaporate.

¹H NMR (CDCl₃, 500.1 MHz): δ = 7.73 (H2, d, ³J(H-H) = 7.5 Hz), 7.62 (H3, d, ³J(H-H) = 7.8 Hz), 7.58 (H7, d, ³J(H-H) = 8.2 Hz), 7.50 (H6, d, ³J(H-H) = 8.5 Hz) ppm; ¹³C NMR (CDCl₃, 125.8 MHz): δ = 141.28 (C4, s), 139.67 (C5, s), 136.94 (C2, s), 133.07 (C1, s), 131.98 (C6, s), 128.72 (C7, s), 126.50 (C3, s) 121.95 (C8, s) ppm; ²⁹Si NMR (CDCl₃, 79.5 MHz): δ = -14.36 ppm; ²⁹Si CP/MAS: δ = -14.7, -15.7 ppm (ν_{rot} = 10 kHz). mp 149 °C.

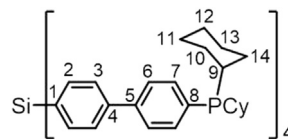
Synthesis of Si(*p*-C₆H₄-*p*-C₆H₄PPh₂)₄ (**2**):



In a 250 ml Schlenk flask, **1** (0.600 g, 0.63 mmol) is dissolved in 75 ml of THF. The solution is cooled to -78 °C and 1.51 ml of 2.5 M ⁿBuLi (3.8 mmol) in hexanes is added dropwise and the solution is stirred for 90 min. Then 0.84 g of ClPPh₂ (3.8 mmol) is added dropwise, the reaction mixture is allowed to warm to room temperature and stirred overnight. The solvent is removed *in vacuo* which results in an oil. The product is precipitated with ethanol and filtered onto a frit under N₂. The powder is washed three more times with 25 ml of ethanol and dried *in vacuo*. The product is obtained as 0.695 g of a white powder (0.50 mmol, yield 80%).

¹H NMR (CDCl₃, 500.1 MHz): δ = 7.72 (H2, d, ³J(H-H) = 7.8 Hz), 7.66 (H6, dd, ³J(H-H) = 7.5 Hz), ⁴J(P-H) = 1.6 Hz), 7.62 (H3, d, ³J(H-H) = 7.4 Hz), 7.39 (H7, t, ³J(H-H) = 7.6 Hz, ³J(P-H) = 7.6 Hz), 7.37 (H10-H12, m) ppm; ¹³C NMR (CDCl₃, 125.8 MHz): δ 141.70 (C4, s), 141.01 (C5, s), 136.92 (C2, s), 134.18 (C7, d, ²J(P-C) = 19.5 Hz), 133.77 (C10, d, ²J(P-C) = 19.5 Hz), 133.69 (C1, s), 132.69 (C8, d, ¹J(P-C) = 18.6 Hz), 130.31 (C9, d, ¹J(P-C) = 21.4 Hz), 128.79 (C12, s), 128.54 (C11, d, ³J(P-C) = 7.0 Hz), 127.15 (C6, d, ³J(P-C) = 6.5 Hz), 126.59 (C3, s) ppm; ³¹P NMR (CDCl₃, 162.0 MHz) -6.11 ppm. mp 125 °C. ESI-MS⁺: [M+1] 1377.37 (96%) and [M+2] 1378.34 (100%) plus decomposition products, calculated 1377.44 (96%), 1378.44 (100%).

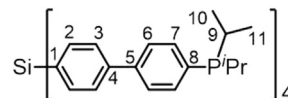
Synthesis of Si(*p*-C₆H₄-*p*-C₆H₄PCy₂)₄ (**3**):



The synthesis of **3** was performed in analogy to the synthesis of **2** described above. Compound **3** was obtained as a white powder in a yield of 93%.

¹H NMR (CDCl₃, 500.1 MHz): δ = 7.75 (H2, d, ³J(H-H) = 8.1 Hz), 7.70 (H3, d, ³J(H-H) = 8.3 Hz), 7.64 (H7, d, ³J(H-H) = 7.8 Hz), 7.56 (H6, dd, ³J(H-H) = 7.3 Hz, ³J(P-H) = 7.3 Hz), 1.98–1.66 (9, 10e, 11e, 13e, 12e, 14e, m), 1.43–0.91 (11a, 13a, 10a, 12a, 14a, m) ppm (Fig. 3); ¹³C NMR (CDCl₃, 125.8 MHz): δ 141.70 (C4, s), 140.91 (C5, s), 136.91 (C2, s), 135.18 (C7, d, ²J(P-C) = 19.1 Hz), 134.02 (C8, d, ¹J(P-C) = 17.7 Hz), 133.05 (C1, s), 126.54 (C3, s), 126.40 (C6, d, ³J(P-C) = 7.4 Hz), 32.49 (C9, d, ¹J(P-C) = 11.2 Hz), 30.01 (C10, d, ²J(P-C) = 15.8 Hz), 28.82 (C14, d, ²J(P-C) = 7.0 Hz), 27.24 (C11, d, ³J(P-C) = 12.6 Hz), 27.00 (C13, d, ³J(P-C) = 7.4 Hz), 26.39 (C12, s) ppm; ³¹P NMR (CDCl₃, 162.0 MHz) 1.92 ppm. mp 117 °C. ESI-MS⁺: [M+1] 1425.78 (96%) and [M+2] 1426.76 (100%) plus decomposition products, calculated 1425.81 (92%), 1426.81 (100%).

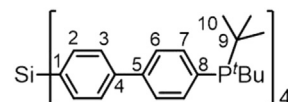
Synthesis of Si(*p*-C₆H₄-*p*-C₆H₄PⁱPr₂)₄ (**4**):



The synthesis of **4** was performed in analogy to the synthesis of **2** described above. Compound **4** was obtained as a white powder in a yield of 64%.

¹H NMR (CDCl₃, 500.1 MHz): δ = 7.75 (H2, d, ³J(H-H) = 8.3 Hz), 7.70 (H3, d, ³J(H-H) = 8.3 Hz), 7.64 (H6, d, ³J(H-H) = 7.8 Hz), 7.57 (H7, dd, ³J(H-H) = 8.0 Hz, ³J(P-H) = 6.6 Hz), 2.16 (H9, m), 1.13 (H10, dd (³J(H-H) = 7.1 Hz, ³J(P-H) = 15.1 Hz), 0.98 (H11, dd (³J(H-H) = 6.9 Hz, ³J(P-H) = 11.6 Hz) ppm; ¹³C NMR (CDCl₃, 125.8 MHz): δ 141.86 (C4, s), 141.12 (C5, s), 136.93 (C2, s), 135.05 (C7, d, ²J(P-C) = 18.5 Hz), 134.06 (C8, d, ¹J(P-C) = 16.0 Hz), 133.10 (C1, s), 126.58 (C3, s), 126.46 (C6, d, ³J(P-C) = 7.6 Hz), 22.79 (C9, d, ¹J(P-C) = 10.9 Hz), 19.86 (C10, d, ²J(P-C) = 18.5 Hz), 18.79 (C11, d, ²J(P-C) = 8.4 Hz) ppm; ³¹P NMR (CDCl₃, 162.0 MHz) 10.54 ppm. ²⁹Si NMR (CDCl₃, 79.5 MHz): δ = -15.3 ppm. mp 205 °C. ESI-MS⁺: [M+1] 1105.51 (100%) and [M+2] 1106.49 (78%) plus decomposition products, calculated 1105.56 (100%), 1106.56 (83%).

Synthesis of Si(*p*-C₆H₄-*p*-C₆H₄P^tBu)₄ (**5**):

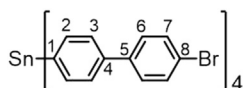


The synthesis of **5** was performed in analogy to the synthesis of **2** described above. Compound **5** was obtained as a white powder in a yield of 75%.

¹H NMR (CDCl₃, 500.1 MHz): δ = 7.78 (H7, dd, ³J(H-H) = 7.6 Hz, ³J(P-H) = 7.6 Hz), 7.75 (H2, d, ³J(H-H) = 7.3 Hz), 7.70 (H3, d, ³J(H-H) = 7.3 Hz), 7.62 (H6, d, ³J(H-H) = 7.6 Hz), 1.24 (H10, d, ³J(P-H) = 11.7 Hz) ppm; ¹³C NMR (CDCl₃, 125.8 MHz): δ 141.80 (C4, s), 141.15 (C5, s), 136.93 (C2, s), 136.90 (C7, d, ²J(P-C) = 15.2 Hz), 136.15 (C8, d, ¹J(P-C) = 22.0 Hz), 133.10 (C1, s), 126.59 (C3, s), 126.13 (C6, d, ³J(P-C) = 8.4 Hz), 32.02 (C9, d, ¹J(P-C) = 20.2 Hz), 30.48 (C10, d, ²J(P-C) = 14.3 Hz); ³¹P NMR (CDCl₃, 162.0 MHz) 38.18 ppm. mp 240 °C (decomp.). ESI-MS⁺: [M+1] 1217.66 (100%) and [M+2] 1218.66 (100%) plus decomposition products, calculated 1217.69 (100.0%),

1218.69 (92.8%).

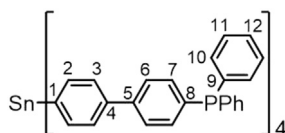
Synthesis of $\text{Sn}(p\text{-C}_6\text{H}_4\text{-}p\text{-C}_6\text{H}_4\text{Br})_4$ (**6**):



In a 500 ml Schlenk flask, 4,4'-dibromobenzene (2.718 g, 8.71 mmol) is dissolved in 300 ml of ether. The solution is cooled to -78°C and 6.25 ml of 1.6 M $^n\text{BuLi}$ (10.0 mmol) in hexanes is added dropwise. After stirring the mixture at room temperature for 90 min, the supernatant is separated from the precipitate via cannula and placed in a different 500 ml Schlenk flask. The flask is cooled to -78°C and 0.20 mL of SnCl_4 (0.442 g, 1.70 mmol) is added dropwise. The reaction mixture is warmed to room temperature and stirred overnight. The solvent is then removed in *vacuo* and the crude product is redissolved in 80 ml of dichloromethane. Flash chromatography is then performed with dichloromethane as the eluent. The solvent is removed in *vacuo* and the powder is washed 3 times with 20 ml of hexanes. Residual solvent is removed in *vacuo* and the product is obtained as white powder in a yield of 29% (0.660 g, 0.49 mmol).

^1H NMR (CDCl_3 , 500.1 MHz): $\delta = 7.74$ (H2, d, $^3J(\text{H-H}) = 8.3$ Hz), 7.63 (H3, d, $^3J(\text{H-H}) = 8.0$ Hz), 7.57 (H7, d, $^3J(\text{H-H}) = 8.8$ Hz), 7.47 (H6, d, $^3J(\text{H-H}) = 8.8$ Hz) ppm; ^{13}C NMR (CDCl_3 , 125.8 MHz): $\delta = 140.95$ (C4, s), 139.75 (C5, s), 137.70 (C2, s), 136.80 (C1, s), 131.98 (C6, s), 128.71 (C7, s), 127.19 (C3, s), 121.88 (C8, s) ppm; ^{119}Sn NMR (CDCl_3 , 149.2 MHz): $\delta = -124.3$ ppm.

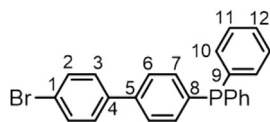
Synthesis of $\text{Sn}(p\text{-C}_6\text{H}_4\text{-}p\text{-C}_6\text{H}_4\text{PPh}_2)_4$ (**7**):



In a 50 ml Schlenk flask, **8** (0.320 g, 0.77 mmol) is dissolved in 10 ml of THF. The solution is cooled to -78°C and 5 ml of THF, together with $^n\text{BuLi}$ (0.77 mmol) and TMEDA (0.97 mmol), is added dropwise while stirring the solution for 5 min. Then SnCl_4 (0.050 g, 0.19 mmol) is added dropwise, the reaction mixture is allowed to warm to room temperature and stirred overnight. The solution is then passed through SiO_2 and the solvent is removed in *vacuo*. The residue is washed with ethanol and the suspension is filtered through a frit under N_2 . The retained powder is washed three more times with 15 ml aliquots of ethanol and dried in *vacuo*. The product is obtained as 0.148 g of a light yellow powder (0.10 mmol, crude yield 52%).

^1H NMR (CDCl_3 , 500.1 MHz): $\delta = 7.75$ (H2, d, $^3J(\text{H-H}) = 7.8$ Hz), 7.66 (H6, dd, $^3J(\text{H-H}) = 7.5$ Hz), $^4J(\text{P-H}) = 1.5$ Hz), 7.63 (H3, d, $^3J(\text{H-H}) = 7.8$ Hz), 7.40 (H7, dd, $^3J(\text{H-H}) = 7.5$ Hz, $^3J(\text{P-H}) = 8.3$ Hz), 7.37 (H10-H12, m) ppm; ^{13}C NMR (CDCl_3 , 125.8 MHz): $\delta = 140.98$ (C4, s), 139.77 (C5, s), 136.92 (C2, s), 134.20 (C7, d, $^2J(\text{P-C}) = 19.6$ Hz), 133.79 (C10, d, $^2J(\text{P-C}) = 19.4$ Hz), 136.82 (C1, s), 137.19 (C8, d, $^1J(\text{P-C}) = 17.4$ Hz), 136.92 (C9, d, $^1J(\text{P-C}) = 25.5$ Hz), 128.81 (C12, s), 128.57 (C11, d, $^3J(\text{P-C}) = 7.0$ Hz), 127.22 (C3, s), 127.16 (C6, d, $^3J(\text{P-C}) = 7.0$ Hz) ppm; ^{31}P NMR (CDCl_3 , 162.0 MHz) -6.12 ppm.

Synthesis of $p\text{-BrC}_6\text{H}_4\text{-}p\text{-C}_6\text{H}_4\text{PPh}_2$ (**8**):



In a 500 ml Schlenk flask, 4,4'-dibromobenzene (1.952 g, 6.26 mmol) is dissolved in 350 ml of ether. The solution is cooled

to -78°C and 4.30 mL of 1.6 M $^n\text{BuLi}$ (6.88 mmol) in hexanes is added dropwise. After allowing the mixture to stir at room temperature for 90 min, the solution is separated from the precipitate via cannula and placed in a different 500 ml Schlenk flask. The flask is cooled to -78°C and 1.12 ml of ClPPh_2 (6.88 mmol) is added. The reaction mixture is warmed to room temperature and stirred overnight. The solvent is then removed in *vacuo* and the crude product is filtered through a frit and washed 3 times with 20 ml of ethanol. The residual ethanol is removed in *vacuo* and the product is obtained as a white powder in a yield of 48% (1.230 g, 2.95 mmol).

^1H NMR (CDCl_3 , 500.1 MHz): $\delta = 7.57$ (H2, d, $^3J(\text{H-H}) = 8.3$ Hz), 7.53 (H6, d, $^3J(\text{H-H}) = 7.8$ Hz), 7.47 (H3, d, $^3J(\text{H-H}) = 8.3$ Hz), 7.39 (H7, dd, $^3J(\text{H-H}) = 7.8$ Hz, $^3J(\text{P-H}) = 8.3$ Hz), 7.37 (H10-12) ppm; ^{13}C NMR (CDCl_3 , 125.8 MHz): $\delta = 140.17$ (C5, s), 139.41 (C4, s), 136.96 (C9, d, $^1J(\text{P-C}) = 10.2$ Hz), 136.75 (C8, d, $^1J(\text{P-C}) = 10.2$ Hz), 134.43 (C7, d, $^2J(\text{P-C}) = 19.5$ Hz), 133.75 (C10, d, $^2J(\text{P-C}) = 19.5$ Hz), 131.93 (C2, s), 128.83 (C3, s), 128.63 (C12, s), 128.56 (C11, d, $^3J(\text{P-C}) = 7.0$ Hz), 126.92 (C6, d, $^3J(\text{P-C}) = 7.0$ Hz), 121.83 (C1, s) ppm; ^{31}P NMR (CDCl_3 , 162.0 MHz) -6.17 ppm.

Immobilization of $\text{Si}(p\text{-C}_6\text{H}_4\text{-}p\text{-C}_6\text{H}_4\text{PPh}_2)_4$ to give **2i**:

Immobilization of **2** on SiO_2 via three phosphonium groups: 2.480 g of rigorously dried SiO_2 is suspended in 10 ml of toluene, and a solution of 0.120 g (0.08 mmol) of **2** in 20 ml of toluene, together with 1.70 g (7.0 mmol) of $\text{Cl}(\text{CH}_2)_3\text{Si}(\text{OEt})_3$ is added. The mixture is heated to 90°C and stirred for 6 d in a gas storage vessel. After cooling to ambient temperature and allowing the silica to settle, the supernatant is decanted. Then the silica is washed with three 25 ml aliquots of toluene and dried in *vacuo*. Since no traces of phosphorus containing substances are found in the supernatant, the surface coverage can be determined to be about 2.9 linker molecules per 100 nm^2 of silica surface. ^{31}P MAS (quantitative): $\delta_{\text{iso}} = 23.5$ (PPh_2Et^+), -5.5 ppm (PPh_2), intensity ratio 3.0:1.3.

Immobilization of $\text{Si}(p\text{-C}_6\text{H}_4\text{-}p\text{-C}_6\text{H}_4\text{PCy}_2)_4$ to give **3i**:

The immobilization procedures for **3i** was analogous to the one described above for **2i**. Surface coverage: 4.7 particles/ 100 nm^2 , ^{31}P MAS: 31.3 ppm (PCy_2Et^+), 1.0 ppm (PCy_2), intensity ratio 3.0:1.5.

Immobilization of $\text{Si}(p\text{-C}_6\text{H}_4\text{-}p\text{-C}_6\text{H}_4\text{P}^i\text{Pr}_2)_4$ to give **4i**:

The immobilization procedure for **4i** was analogous to the one described above for **2i**. Surface coverage of 4.0 particles/ 100 nm^2 , ^{31}P MAS: 37.4 ppm ($\text{P}^i\text{Pr}_2\text{Et}^+$), 10.4 ppm (P^iPr_2), intensity ratio 3.0:1.1.

Generating Immobilized Catalysts **2iRh**, **3iRh** and **4iRh**:

The linker-modified silica **2i-4i** are suspended in 20 ml of toluene and combined with a solution of $\text{ClRh}(\text{PPh}_3)_3$ (slight excess, 1.1 mmol per 1 mmol of linker molecule) in 10 ml of toluene. After stirring for 5 h at ambient temperature, the silica is allowed to settle and the supernatant is decanted. The silica is washed with three 15 ml aliquots of toluene to remove excess $\text{ClRh}(\text{PPh}_3)_3$ and PPh_3 , and dried in *vacuo*. The surface coverages are calculated based on the fact that no signals for uncoordinated PR_2 ($\text{R} = \text{Ph}, \text{Cy}, ^i\text{Pr}$) groups are visible in the ^{31}P CP/MAS spectra, and the knowledge of the linker surface coverages. For **2iRh** 2.9 Rh complexes, **3iRh** 4.7 Rh complexes, and for **4iRh** 4.0 Rh complexes are bound on 100 nm^2 of silica surface.

9. General hydrogenation procedure

Immobilized catalyst **2iRh** (240 mg, containing 10 mg of Wilkinson's catalyst, corresponding to 0.010 mmol Rh) is suspended in 5 ml of toluene in a Schlenk flask. The mixture appears opaque and orange/pink in color. The flask is then attached to the hydrogenation apparatus described earlier [12d] and 1 mmol of 1-dodecene, dissolved in toluene (5 ml), is added to the suspension of **2iRh** with a syringe through the stopcock. Subsequently the suspension is stirred vigorously and the hydrogen consumption is monitored.

After complete substrate conversion the catalyst is allowed to settle, the supernatant is removed via syringe and the material is washed three times with 5 ml of toluene. To start the second and following cycles, fresh toluene is added and the described procedure is repeated.

Competing financial interest

The authors declare no competing financial interest.

Acknowledgment

This material is based on work supported by the National Science Foundation (CHE-1300208). Furthermore, we thank Kevin Dong and Scott Leyendecker for contributing some experiments.

Supplementary material

Supplementary data related to this article can be found at <http://dx.doi.org/10.1016/j.jorganchem.2017.03.034>

References

- J.A. Gladysz, *Pure Appl. Chem.* 73 (2001) 1319–1324.
- Selected references: (a) J.A. Gladysz, D.P. Curran, I.T. Horvath, *Handbook of Fluorous Chemistry*, Wiley-VCH Verlag GmbH & Co. KGaA, 2004; (b) J.J.J. Juliette, D. Rutherford, I.T. Horváth, J.A. Gladysz, *J. Am. Chem. Soc.* 121 (1999) 2696–2704; (c) M.-A. Guillevis, C. Rocaboy, A.M. Arif, I.T. Horváth, J.A. Gladysz, *Organometallics* 17 (1998) 707–717; (d) J.J.J. Juliette, J.A. Gladysz, I.T. Horváth, *Angew. Chem. Int. Ed.* 36 (1997) 1610–1612.
- L.V. Dinh, J.A. Gladysz, *Angew. Chem. Int. Ed.* 44 (2005) 4095–4097.
- Selected books and reviews: (a) P. Barbaro, F. Liguori (Eds.), *Heterogenized Homogeneous Catalysts for Fine Chemicals Production*, Springer, Heidelberg, 2010; (b) J. Blümel, *Coord. Chem. Rev.* 252 (2008) 2410–2423; (c) F.R. Hartley, *Supported Metal Complexes*, D. Reidel, Publ. Co., Dordrecht, The Netherlands, 1985; (d) D.E. DeVos, I.F.J. Vankelecom, P.A. Jacobs (Eds.), *Chiral Catalyst Immobilization and Recycling*, Wiley-VCH, Weinheim, 2000; (e) G. Rothenberg, *Catalysis: Concepts and Green Applications*, Wiley-VCH, Weinheim, 2008.
- R. Silbernagel, A. Diaz, E. Steffensmeier, A. Clearfield, J. Blümel, *J. Mol. Catal. A Chem.* 394 (2014) 217–223.
- C. Merckle, J. Blümel, *Chem. Mater.* 13 (2001) 3617–3623.
- Merck silica 40, Average Particle Size 0.063–0.2 mm, Specific Surface Area 750 m²/g, Average Pore Diameter 40 Å.
- (a) J. Blümel, *J. Am. Chem. Soc.* 117 (1995) 2112–2113; (b) K.D. Behringer, J. Blümel, *J. Liq. Chromatogr.* 19 (1996) 2753–2765.
- (a) E.F. Vansant, P. VanDer Voort, K.C. Vrancken, *Characterization and Chemical Modification of the Silica Surface*, Elsevier, Amsterdam, 1995; (b) R.P.W. Scott, *Silica Gel and Bonded Phases*, John Wiley and Sons, New York, 1993.
- (a) K.D. Behringer, J. Blümel, *Inorg. Chem.* 35 (1996) 1814–1819; (b) S. Reinhard, P. Soba, F. Rominger, J. Blümel, *Adv. Synth. Catal.* 345 (2003) 589–602; (c) F. Piester, R. Fetouaki, M. Bogza, T. Oeser, J. Blümel, *Chem. Commun.* (2005) 1481–1483.
- (a) T. Posset, J. Blümel, *J. Am. Chem. Soc.* 128 (2006) 8394–8395; (b) T. Posset, J. Guenther, J. Pope, T. Oeser, J. Blümel, *Chem. Commun.* 47 (2011) 2059–2061; (c) J.C. Pope, T. Posset, N. Bhuvanesh, J. Blümel, *Organometallics* 33 (2014) 6750–6753.
- (a) J. Guenther, J. Reibenspies, J. Blümel, *Adv. Synth. Catal.* 353 (2011) 443–460; (b) C. Merckle, J. Blümel, *Top. Catal.* 34 (2005) 5–15; (c) C. Merckle, J. Blümel, *Adv. Synth. Catal.* 345 (2003) 584–588; (d) C. Merckle, S. Haubrich, J. Blümel, *J. Organomet. Chem.* 627 (2001) 44–54.
- J.A. Osborn, F.H. Jardine, J.F. Young, G. Wilkinson, *J. Chem. Soc. A Inorg. Phys. Theor.* (1966) 1711–1732.
- T. Posset, F. Rominger, J. Blümel, *Chem. Mater.* 17 (2005) 586–595.
- (a) J. Blümel, *Inorg. Chem.* 33 (1994) 5050–5056; (b) J. Sommer, Y. Yang, D. Rambow, J. Blümel, *Inorg. Chem.* 43 (2004) 7561–7563.
- Y. Yang, B. Beele, J. Blümel, *J. Am. Chem. Soc.* 130 (2008) 3771–3773.
- B. Beele, J. Guenther, M. Perera, M. Stach, T. Oeser, J. Blümel, *New J. Chem.* 34 (2010) 2729–2731.
- (a) , in: first ed., in: J.G. de Vries, C.J. Elsevier (Eds.), *The Handbook of Homogeneous Hydrogenation*, vols. 1–3, Wiley-VCH, Weinheim, 2007; (b) G. Ertl, H. Knözinger, F. Schüth, J. Weitkamp (Eds.), *Handbook of Heterogeneous Catalysis*, second ed., Wiley-VCH, Weinheim, 2008; (c) M. Wende, R. Meier, J.A. Gladysz, *J. Am. Chem. Soc.* 123 (2001) 11490 (and lit. cited therein); (d) *Adv. Synth. Catal.* 345 (2003) vols. 1+2, Special Issue on Hydrogenation, including, e.g.: W.S. Knowles, *Adv. Synth. Catal.* 345 (2003) 3; R. Noyori, *Adv. Synth. Catal.* 345 (2003) 15; T. Imamoto, *Adv. Synth. Catal.* 2003, 345, 79; (e) D.M. Heinekey, A. Lledós, J.M. Lluch, *Chem. Soc. Rev.* 33 (2004) 175–182.
- (a) D. Rutherford, J.J.J. Juliette, C. Rocaboy, I.T. Horváth, J.A. Gladysz, *Catal. Today* 42 (1998) 381–388; (b) K. Kromm, B.D. Zwick, O. Meyer, F. Hampel, J.A. Gladysz, *Chemistry* 7 (2001) 2015–2027; (c) K. Kromm, P.L. Osburn, J.A. Gladysz, *Organometallics* 21 (2002) 4275–4280; (d) T. Soós, B.L. Bennett, D. Rutherford, L.P. Barthel-Rosa, J.A. Gladysz, *Organometallics* 20 (2001) 3079–3086.
- (a) M. Zhang, Y.-P. Chen, M. Bosch, T. Gentle, K. Wang, D. Feng, Z.U. Wang, H.-C. Zhou, *Angew. Chem. Int. Ed.* 53 (2014) 815–818; (b) D. Feng, K. Wang, Z. Wei, Y.-P. Chen, C.M. Simon, R.K. Arvapally, R.L. Martin, M. Bosch, T.-F. Liu, S. Fordham, D. Yuan, M.A. Omary, M. Haranczyk, B. Smit, H.-C. Zhou, *Nat. Commun.* (2014) 5723–5732; (c) L. Wen, P. Cheng, W. Lin, *Chem. Sci.* 3 (2012) 2288–2292; (d) L. Ma, A. Jin, Z. Xie, W. Lin, *Angew. Chem. Int. Ed.* 48 (2009) 9905–9908.
- (a) A. Fraccarollo, L. Canti, L. Marchese, M. Cossi, *Langmuir* 30 (2014) 4147–4156; (b) M. Cossi, G. Gatti, L. Canti, L. Tei, M. Errahali, L. Marchese, *Langmuir* 28 (2012) 14405–14414; (c) H. Yu, C. Shen, M. Tian, J. Qu, Z. Wang, *Macromolecules* 45 (2012) 5140–5150; (d) W. Lu, D. Yuan, D. Zhao, C.I. Schilling, O. Plietzsch, T. Müller, S. Bräse, J. Guenther, J. Blümel, R. Krishna, Z. Li, H.-C. Zhou, *Chem. Mater.* 22 (2010) 5964–5972.
- (a) J. You, G. Li, Z. Wang, *RSC Adv.* 2 (2012) 9488–9494; (b) S.-O. Kim, Q. Zhao, K. Thangaraju, J.J. Kim, Y.-H. Kim, S.-K. Kwon, *Dyes Pigments* 90 (2011) 139–145.
- (a) L. Wang, D. Wang, H. Wang, S. Feng, *J. Organomet. Chem.* 767 (2014) 40–45; (b) I. Eryazici, O.K. Farha, O.C. Compton, C. Stern, J.T. Hupp, S.T. Nguyen, *Dalton Trans.* 40 (2011) 9189–9193; (c) P.K. Iyer, S. Wang, *Tetrahedron Lett.* 47 (2006) 437–439; (d) S. Wang, W.J. Oldham Jr., R.A. Hudack Jr., G.C. Bazan, *J. Am. Chem. Soc.* 122 (2000) 5695–5709; (e) D.-R. Bai, S. Wang, *Organometallics* 23 (2004) 5958–5966; (f) Q. Shen, S. Ye, G. Yu, P. Lu, Y. Liu, *Synth. Met.* 158 (2008) 1054–1058.
- (a) C.Y. Yang, S. Wang, M.R. Robinson, G.C. Bazan, A.J. Heeger, *Chem. Mater.* 13 (2001) 2342–2348; (b) A. Pegenau, T. Hegmann, C. Tschierske, S. Diele, *Chem. - Eur. J.* 5 (1999) 1643–1660; (c) M. Lequan, C. Branger, J. Simon, T. Thami, E. Chauchard, A. Persoons, *Adv. Mat. (Weinheim, Ger.)* 6 (1994) 851–853; (d) S. Murphy, X. Yang, G.B. Schuster, *J. Org. Chem.* 60 (1995) 2411–2422; (e) E.S. Blake, W.C. Hammann, J.W. Edwards, T.E. Reichard, M.R. Ort, *J. Chem. Eng. Data* 6 (1961) 87–98.
- (a) C.A. Fyfe, *Solid-state NMR for Chemists*, C.F.C. Press, Guelph, Canada, 1983; (b) T.M. Duncan, *A Compilation of Chemical Shift Anisotropies*, Farragut Press, Chicago, IL, 1990; (c) S. Reinhard, J. Blümel, *Magn. Reson. Chem.* 41 (2003) 406.
- (a) K.J. Cluff, J. Blümel, *Organometallics* 35 (2016) 3939–3948; (b) K.J. Cluff, J. Blümel, *Chem. Eur. J.* 22 (2016) 16562–16575; (c) K.J. Cluff, J. Blümel, *Organometallics* 33 (2014) 2671–2680; (d) K.J. Cluff, M. Schnellbach, C.R. Hilliard, J. Blümel, *J. Organomet. Chem.* 744 (2013) 119–124.
- (a) S. Kotha, V.R. Shah, *Amino Acids* 35 (2008) 83–88; (b) B. Liu, T.T.T. Dan, G.C. Bazan, *Adv. Funct. Mater.* 17 (2007) 2432–2438; (c) Y. Takeuchi, M. Nishikawa, H. Hachiya, H. Yamamoto, *Magn. Reson. Chem.* 43 (2005) 662–664; (d) T. Alaviuhkola, J. Bobacka, M. Nissinen, K. Rissanen, A. Ivaska, J. Pursiainen, *Chem. Eur. J.* 11 (2005) 2071–2080; (e) X.-M. Liu, C. He, X.-T. Hao, L.-W. Tan, Y. Li, K.S. Ong, *Macromolecules* 37 (2004) 5965–5970; (f) B.N. Biddle, J.S. Gray, *Appl. Organomet. Chem.* 3 (1989) 537–543; (g) W.C. Schumb, J. Ackerman Jr., C.M. Saffer Jr., *J. Am. Chem. Soc.* 60 (1938) 2486–2488.
- (a) A. Nagaki, N. Takabayashi, Y. Tomida, J.-I. Yoshida, *Beilstein, J. Org. Chem.* 5 (2009) 16–27; (b) A. Nagaki, N. Takabayashi, Y. Tomida, J.-I. Yoshida, *Org. Lett.* 10 (2008) 3937–3940; (c) S.J. Dolman, F. Gosselin, P.D. O'Shea, I.W. Davies, *Tetrahedron* 62 (2006) 5092–5098.
- Y. Yang, *Doctoral thesis, University of Heidelberg*, 2007.
- C.F. Nising, U.K. Schmid, M. Nieger, S. Bräse, *J. Org. Chem.* 69 (2004) 6830–6833.
- CCDC 1527673 contains the supplementary crystallographic data for this

- compound. This data can be obtained free of charge from The Cambridge Crystallographic Data Centre. The unit cell parameters are $a = 16.7257(9)$, $b = 16.7257(9)$, $c = 7.1979(4)$. The space group is $P-4$.
- [32] J. Stahl, J.C. Bohling, E.B. Bauer, T.B. Peters, W. Mohr, J.M. Martin-Alvarez, F. Hampel, J.A. Gladysz, *Angew. Chem. Int. Ed.* **41** (2002) 1871–1876.
- [33] R.J. Hinch, J. Krc, *Anal. Chem.* **29** (1957) 1550–1551.
- [34] J. Schraml, M. Čapka, V. Blechta, *Magn. Reson. Chem.* **30** (1992) 544–547.
- [35] F.H. Köhler, N. Hertkorn, J. Blümel, *Chem. Ber.* **120** (1987) 2081–2082.
- [36] C.R. Hilliard, S. Kharel, K.J. Cluff, N. Bhuvanesh, J.A. Gladysz, J. Blümel, *Chem. Eur. J.* **20** (2014) 17292–17295.